

IMPLEMENTATION OF A NUMERICAL MODEL FOR THE CYCLOIDAL ROTOR AERODYNAMICS

Dekterev Ar.A. , Dekterev A.A. , Sentyabov A.V. ¹, Filimonov S.A. 

Abstract The paper presents a numerical model and calculations of the aerodynamics of a cycloidal rotor. The cycloidal rotor is a rotor consisting of blades located parallel to the rotor axis, and in addition to rotation, they perform a swing around their own axis, which allows the blade to maintain positive angles of attack and generate lift force in both its upper and lower positions. The numerical model of the flow around the rotor was based on computational fluid dynamics methods and described by the viscous, turbulent incompressible flow of air through the rotor. Discretization of the transfer equations was carried out using the control volume method on three-dimensional meshes with hexahedral cells, while the movement of the blades was taken into account using the sliding mesh method. Validation of the model showed good agreement with known experimental data. Scaling the problem parameters confirmed the self-similarity of the dimensionless characteristics of the rotor in the studied range of Reynolds numbers.

Key words: cycloidal rotor, CFD, sliding meshes, thrust.

AMS Mathematics Subject Classification: 76-10.

DOI: 10.32523/2306-6172-2025-13-2-43-49

1 Introduction

The cycloidal rotor consists of several blades that perform a rotational movement around the rotor axis and, in addition to this, a swing motion around its axis, so that the blades experience positive angles of attack in both the upper and lower positions of the cycle. Such a rotor can be used both as a propulsion device for aircraft or ships, and as a vertical wind turbine [1]. Its advantage is that changing the amplitude and phase of the cyclic pitch of the blade can be used to change the magnitude and direction of the thrust vector generated by the rotor. Since the thrust vector of cycloidal rotor can be set almost instantly in any direction perpendicular to the axis of rotation, cycloidal rotor based vehicles may demonstrate better maneuverability and a greater range of inclination angles to the horizon. Additionally, the higher utilization rate of the rotor's sweep area makes it more compact than a conventional propeller, which allows it to get closer to vertical walls etc.

Aircraft based on a cyclic engine have been proposed since the beginning of the 20th century in the projects of Sverchkov (1909), Brooks (1920), Caldwell, Rohrbach (1933) and Wheatley (1935), Sharpe (1980) and others. In the 21st century, several projects of this vehicle have appeared such as projects of Seoul National University (South Korea), the National University of Singapore, the Bosch Aerospace group (Germany), the D-Dalus company (Austria); the Moble Benedict team (University of Maryland), etc. In these projects, it was possible to build working prototypes of the vehicle. In the papers [2, 3] of the CROP project group, the influence of various factors on the characteristics of a cycloidal rotor was studied. In the work [4], the results of the calculated optimization of the blade profile shape are presented, as a result of which a profile close to NACA0016 was obtained. In [5], the influence of the profile

¹Corresponding Author.

pitch angle on the power characteristics of the rotor was investigated. Numerical modeling of the aerodynamics of cycloidal rotors was used to evaluate the characteristics of the aircraft in [6, 7, 8].

To provide the characteristics of vehicles based on a cycloidal rotor under various conditions, further research is required using both experimental and numerical methods. The main goal of this work is to develop and test a numerical model of a cyclic rotor that can be used for comprehensive computational and experimental studies of various aspects of the rotor aerodynamics and improvement of its characteristics. For this purpose, validation based on the works of other authors, the development of a basic model of an experimental rotor developed at the Institute of Thermophysics of the Siberian Branch of the Russian Academy of Sciences, and a study of the rotor characteristics when scaling its parameters were carried out.

2 The problem description

The movement diagram of the cycloidal rotor blade is shown in Fig. 1, on which points O and P are stationary, and connections R and L provide rotation and swing of the blade. The blade rotates relative to the rotor axis, with the origin at point O , and at the same time is capable of rotating around its own axis. The relative angle θ between the chord line of the blade and the tangential direction of the rotor is called the pitch angle of the blade. The pitch angle changes periodically during the rotation cycle, depending on the azimuthal position of the blade Ψ . Angle ϵ specifies the direction of thrust of the cycloidal rotor, and the magnitude of eccentricity e specifies the maximum rotation angles of the blades.

The pitch angle of the blade depending on its azimuthal position can be found by geometric scheme (Fig. 1): $\theta = \pi/2 - \alpha$ where $\alpha = \alpha_1 + \alpha_2$. The distance a , the angle α_1 and the length of the rod L , can be represented using trigonometric expressions: $a^2 = e^2 + R^2 - 2eR \cos(\Psi + \epsilon + \pi/2)$, $\frac{1}{e} \sin(\alpha_1) = \frac{1}{a} \sin(\Psi + \epsilon + \pi/2) = \frac{1}{a} \cos(\Psi + \epsilon)$, $L^2 = a^2 + d^2 - 2ad \cos(\alpha_2)$, where R is radius of rotation of the blade, ϵ is angle of eccentric position, e is eccentricity value.

By combining the previous expressions, we can obtain the dependence of the instantaneous blade pitch angle on the azimuthal position of the blade:

$$\theta(\Psi) = \frac{\pi}{2} - \arcsin \left[\frac{e}{a} \cos(\Psi + \epsilon) \right] - \arccos \left[\frac{a^2 + d^2 - L^2}{2ad} \right]$$

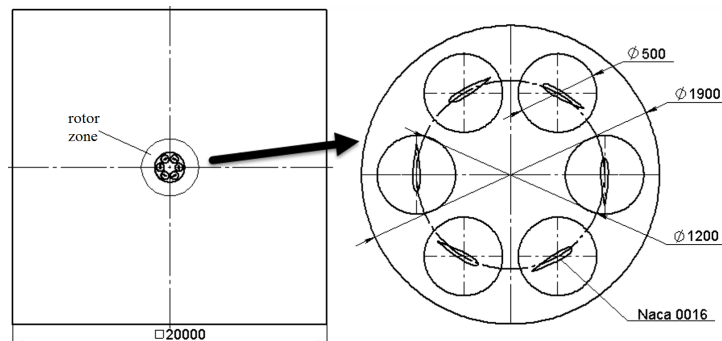
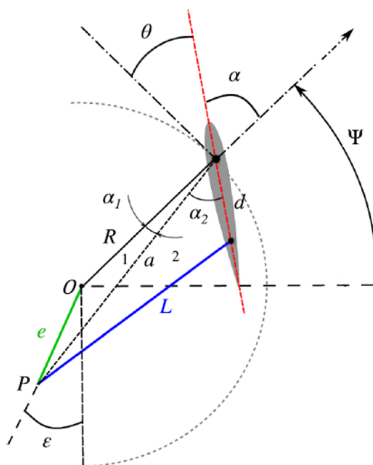


Figure 1: Scheme of the movement of a cycloidal rotor blade [2]

Figure 2: Scheme of the computational domain

3 The numerical model

The complex movement of the blades of a cycloidal rotor requires the implementation of a special methods for calculating the aerodynamics of the rotor, which were carried out by means of Ansys Fluent software package. An example of the geometry of the cycloidal rotor model is shown in Fig. 2. The calculated geometry consisted of the following parts:

1. Fixed zone of surrounding air.
2. The rotor zone, which is calculated in a rotating reference frame. Rotation is set at a constant frequency.
3. Blade zones, which perform a swinging motion relative to the center of the blade attachment and rotate along with the entire rotor. The movement of the blade zone was specified by a special law (5) based on the kinematic diagram (Fig. 1). The interaction between the blade and rotor zones was specified using the sliding mesh method.

The aerodynamics of the rotor were calculated within a model of incompressible viscous turbulent flow in an unsteady formulation. The time step was chosen to correspond to approximately 1° of rotor rotation. Turbulence was modeled using the two-parameter $k-\omega$ SST model [9]. The computational grid was constructed using a multi-block principle of hexahedral cells. Discretization of transport equations was carried out by the finite volume method [10, 11]. The connection between the velocity field and pressure was carried out using the SIMPLEC algorithm [10, 11].

The main characteristics of the rotor are thrust F , (N), which is the vertical component of the force acting on the rotor blades from the flow, and the power P , (W) wasted by the rotor to overcome aerodynamic drag forces. Aerodynamic power P can be approximately determined by the formula $P = M \cdot \omega$, where M is the total moment of pressure forces and friction forces on the rotor blades (N·m), ω is the rotor rotation speed (rad/s). However, this approach does not take into account the power of air drag forces directed against the swing motion of the blades (it is transmitted to the rotor shaft through control rods, which is not taken into account in the aerodynamic calculation). A more accurate approach is to calculate the total power of aerodynamic forces acting on the entire total surface of the blades:

$$P = \int_S (p\mathbf{V})\mathbf{n}dS - \int_S \tau_w \mathbf{V}dS$$

where p is the pressure on the blade surface (Pa), \mathbf{V} is the velocity vector of a point on the blade surface (m/s), τ_w is the vector of tangential stresses acted to the blade surface (Pa·s), dS is the area of the blade surface element (m^2), \mathbf{n} is the normal vector to the surface of the blade (towards the fluid), integration is performed over the entire surface area of the blades.

4 Validation

For validation of the model, experimental data on a cycloidal rotor from the paper [2] were used. The scheme is presented in Fig. 2. The geometric parameters of the experimental rotor are given in Tab. 1. For comparison with the experiment, a mode with a rotor rotational speed of 918 rpm was chosen. The air density was $\rho = 1.225 \text{ kg/m}^3$. The parameters of the computational grid are shown in Tabs. 2, 3, and the picture of grid No 1 is shown in Fig. 3. The meshes were detailed in the blades zones. An example of the calculated velocity field is shown in Fig. 4.

For comparison, calculations were also carried out on 2D meshes. However, in the 3D cases reaching the steady state occurs much faster, in 5 - 7 revolutions. The calculations show a significant advantage of the 3D model over the 2D one with comparable computer time

Table 1: Rotor parameters [2]

| | |
|------------------------|---------------|
| airfoil profile | NACA0016 |
| length | 1.2 m |
| chord | 0.3 m |
| rotor diameter | 1.2 m |
| pitch angles | -39°... + 36° |
| number of blades | 6 |
| rotor rotational speed | 918 rpm |

Table 2: Meshes parameters, 2D

| mesh No | cells number | y_+ on the blade |
|---------|--------------|--------------------|
| 1 | 72000 | 550 |
| 2 | 287000 | 3 |
| 3 | 90000 | 43 |
| 4 | 350000 | 15 |

Table 3: Meshes parameters, 3D

| mesh No | cells number | Number of nodes along the blade span | y_+ on the blade |
|---------|--------------|--------------------------------------|--------------------|
| 1 | 800 000 | 20 | 30 - 100 |
| 2 | 1 000 000 | 20 | 2 - 15 |
| 3 | 1 760 000 | 20 | 2 - 60 |

Table 4: Comparison of calculated rotor parameters with experimental data, 2D meshes

| mesh, No | thrust, N | discrepancy | Power, kW | discrepancy |
|------------|-----------|-------------|-----------|-------------|
| 1 | 2071 | 4.5% | 75 | +17% |
| 2 | 2194 | 11% | 52 | -18% |
| 3 | 2154 | 9% | 54 | -20% |
| 4 | 2139 | 8% | 47 | -27% |
| Experiment | 1981 | | 64 | |

Table 5: Comparison of calculated rotor parameters with experimental data, 3D meshes

| mesh, No | thrust, N | discrepancy | Power, kW | discrepancy |
|------------|-----------|-------------|-----------|-------------|
| 1 | 1942 | -2% | 62 | -3% |
| 2 | 1945 | -2% | 60 | -7% |
| 3 | 1970 | -1% | 56 | -13% |
| Experiment | 1981 | | 64 | |

Table 6: Aerodynamic parameters of a cycloidal rotor depending on rotation speed

| rotation speed (rpm) | f_F | f_P | efficiency (kgF/kW) |
|----------------------|-------|-------|---------------------|
| 900 | 0.260 | 0.131 | 7.16 |
| 1000 | 0.259 | 0.129 | 6.55 |
| 1100 | 0.263 | 0.131 | 5.91 |

Table 7: Aerodynamic parameters of a cycloidal rotor depending on linear scale factor

| scale factor | rotation speed (rpm) | f_F | f_P | efficiency (kgF/kW) |
|--------------|----------------------|-------|-------|---------------------|
| 0.25 | 4000 | 0.245 | 0.141 | 5.637 |
| 0.5 | 2000 | 0.254 | 0.136 | 6.080 |
| 1 | 1000 | 0.259 | 0.129 | 6.553 |
| 2 | 500 | 0.271 | 0.129 | 6.840 |

costs. Although a 2D grid contains fewer cells and requires less time to calculate each time step, due to the reduced dissipation of large vortices in such a formulation reaching a steady state takes much longer: 120 revolutions in 2D formulation versus 6 revolutions in a 3D one. In this case, the accuracy of the 2D calculation is up to 10% for thrust and about 20% for power (Tab. 4). At the same time, three-dimensional calculations with wall resolution show good accuracy: 2% for thrust and 3P'BT"13% for power (Tab. 5).

5 Results of the simulation

Based on the results of validation calculations, a model of the aerodynamics of a 5-blades cycloidal rotor, developed at the Institute of Thermophysics SB RAS, was built. In this case, the blade pitch angle θ varies in the range from $+36$ to -39° . The most important rotor parameters include thrust, power and efficiency. In addition, numerical modeling makes it possible to estimate the aerodynamic forces and moments applied to an individual blade in the rotor.

Fig. 5 shows a typical computational grid. The computational domain has a rectangular shape; the distance between the boundaries of the computational domain and the rotor is about 15 diameters. To speed up three-dimensional calculations of the rotor, a symmetric formulation of the problem was used. A constant pressure was set at all external boundaries of the computational domain, and the velocity was determined by linear extrapolation from the internal points of the domain. The movement of the rotor zone relative to the rest of the computational domain and the blades relative to the rotor was implemented using the sliding mesh approach. At the boundaries of the rotating subdomains, a grid interface was created for the exchange of information with the parts of the computational domain. The time step was equal to $\Delta t = T/360$, where $T = 2\pi/\omega$, which corresponds to a turn of the rotor by 1° .

Similar to drag and lift coefficients, we represent the thrust and power of a cycloidal rotor in the form of the following dimensionless dependencies based on linear blades velocity $R\omega$ and total reference area of the blades NlC :

$$F = \rho NlC (R\omega)^2 f_F(e, \delta, N, C/R, \dots), \quad P = \rho NlC (R\omega)^3 f_P(e, \delta, N, C/R, \dots), \quad (1)$$

where F is propulsion thrust, N is number of the blades, ρ is air density, l is the span length of the blades, C is the blade chord, R is radius of rotation of the blades, ω is rotational speed, P is power to overcome air drag forces, f_F, f_P are dimensionless functions of the rotor configuration, which may depend on such parameters as foil profile, blade pitch angles θ , which are specified by the eccentricity e , and the length of the rod L , the number of rotor blades N , the relative chord of the blade C/R , etc.

The calculation was carried out for three rotational speeds of 900, 1000, and 1100 *rpm*. The calculated parameters of the rotor are given in Tab. 6. As can be seen, the calculation results scale well with increasing linear speed of the blade. As follows from formulas (1), the efficiency of the rotor decreases with increasing linear speed of the blade.

During the CFD calculation, the aerodynamic moment on a single blade relative to its point of rotation was obtained. Fig. 6a shows the blade pitch angle and torque as a function of its angular position. Fig. 6b illustrates the calculated forces for a single blade as a function of its angular position.

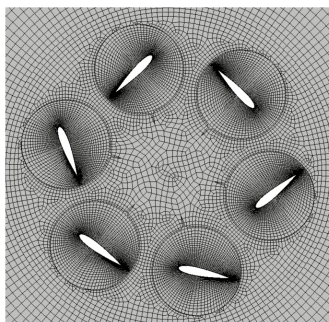


Figure 3: The mesh in central cross-section (800 000 cells)

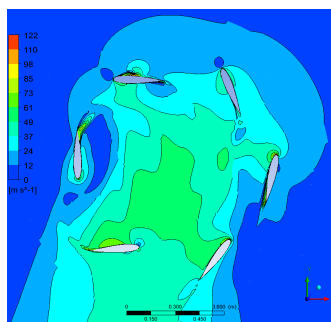


Figure 4: Instantaneous field of velocity magnitude (mesh No 3)

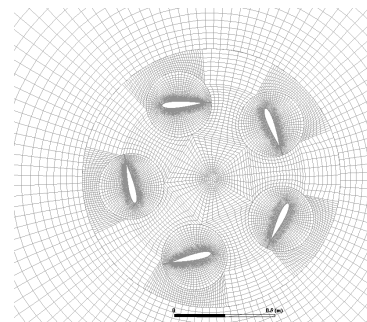


Figure 5: Computational mesh

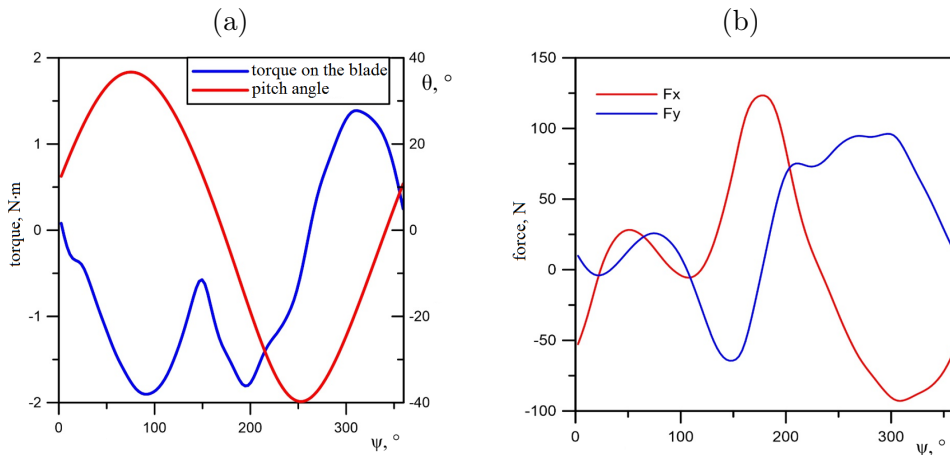


Figure 6: (a) the pitch angle of the blade and the torque on the blade relative to its point of attachment depending on the angular position, (b) forces F_x and F_y for a single blade depending on its angular position

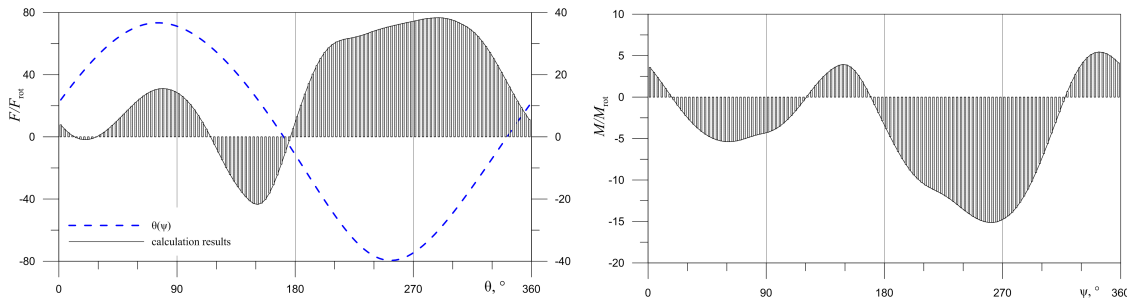


Figure 7: Dependence of the vertical component of aerodynamic forces (upper graph) and the torque relative to the axis of the rotor (lower plot). A positive force means an upward direction (towards the thrust), negative torque value means a torque against the rotation speed.

To study the influence of the linear scale factor, rotors of different diameters were considered, respectively 0.25, 0.5, 1 and 2 diameters. Other linear dimensions, such as blade span length, blade chord, etc., varied in proportion to the rotor diameter. The linear speed of the blade remained constant for all cases; therefore, the rotation frequency varied in inverse proportion to the diameter. As a result of calculations, it was found that the rotor efficiency increases with increasing rotor scale (Tab. 7).

As it rotates around the rotor axis, the blade passes through different flow conditions and experiences significantly different influences from the flow. Fig. 7 shows the results of calculating the forces applied to a single blade in a rotor consisting of five blades. As can be seen from the plot, the main part of the rotor lift force is created when the blade passes the lower half of the revolution. This part of the cycle also accounts for the largest share of the torque on the rotor. In addition, part of the lift force is created when passing the upper point of the revolution near the angular position $\Psi = 90^\circ$.

6 Conclusions

Thus, a numerical model of the aerodynamics of cycloidal rotor was built based on the CFD approach. The validation carried out and comparison with known experimental data show a significant advantage of the three-dimensional model over the two-dimensional one in terms of calculation accuracy with comparable computer time costs. Calculations of a cycloidal rotor

show the constant characteristics in dimensionless form when scaling both the rotor rotation speed and its linear scales. As the blade rotates through a full revolution, it generates most of the lift force (rotor thrust) in the lower half of the cycle in the range of 180 to 360 ° angular position, and some more near the 90 ° angular position. This means that the blade effectively uses the entire swept area of the rotor, which, being a rectangle makes it possible to create a cycloidal rotor for air vehicles that is more compact than a helicopter rotor.

Acknowledgement

The study was carried out under state contract with IT SB RAS 124062400029-2

References

- [1] Dekterev, D. A., Dekterev, A. A., Lobasov, A. S., Platonov, D. V., Sentyabov, A. V. (2019). *Simulation of orthogonal rotors with dynamic pitching blades*, Journal of Physics: Conference Series, 1382(1), 012129. <https://doi.org/10.1088/1742-6596/1382/1/012129>
- [2] Xisto, C. M., Han, J., Van Dam, C. P., Bower, G. C. (2017). *Parametric Analysis of a Large-Scale Cycloidal Rotor in Hovering Conditions*, Journal of Aerospace Engineering, 30(1), 04016066. [https://doi.org/10.1061/\(ASCE\)AS.1943-5525.0000669](https://doi.org/10.1061/(ASCE)AS.1943-5525.0000669)
- [3] Xisto, C. M., Pascoa, J. C., Trancossi, M. (2016). *Geometrical Parameters Influencing the Aerodynamic Efficiency of a Small-Scale Self-Pitch High Solidity VAWT*, Journal of Solar Energy Engineering, 138(2). <https://doi.org/10.1115/1.4032794>
- [4] Tang, J., Hu, Y., Song, B. *Unsteady aerodynamic optimization of airfoil for cycloidal propellers based on surrogate model*, Journal of Aircraft, 54(6), 2222PIP,БЪН2232. <https://doi.org/10.2514/1.C033649>
- [5] Yun, C. Y., Park, K., Lee, H. Y., Jung, J. S., Hwang, I. S. (2007). *Design of a new unmanned aerial vehicle cyclocopter*, Journal of the American Helicopter Society, 52(1), 24PIP,БЪН35. <https://doi.org/10.4050/JAHS.52.24>
- [6] Hu, Y., Wang, G., Zhang, H., Liu, J., Yang, X., Zhu, B. (2017). *The effects of advance ratio and blade number on the forward flight efficiency of cycloidal rotor*, In 55th AIAA Aerospace Sciences Meeting, AIAA SciTech Forum. <https://doi.org/10.2514/6.2017-0096>
- [7] Benedict, M., Ramasamy, M., Chopra, I. (2010). *Improving the aerodynamic performance of micro-air-vehicle-scale cycloidal rotor: An experimental approach*, Journal of Aircraft, 47(4), 1117PIP,БЪН1125. <https://doi.org/10.2514/1.47317>
- [8] Leger, J., Parscoa, J., Xisto, C. (2013). *Analytical modeling of a cyclorotor in forward flight*, (SAE Technical Paper No. 2013-01-2271). SAE International. <https://doi.org/10.4271/2013-01-2271>.
- [9] Menter, F. R. (1994). *Two-equation eddy-viscosity turbulence models for engineering applications*, AIAA Journal, 32(8), 1598PIP,БЪН1605. <https://doi.org/10.2514/3.12149>.
- [10] Ferziger, J. H., PeriP'БЪЎ, M. (2002). *Computational Methods for fluid dynamics*, Springer-Verlag, Berlin, Heidelberg.
- [11] Patankar S. (1980). *Numerical Heat Transfer and Fluid Flow*, Hemisphere Publishing Corporation.

Dekterev Artem,
Kutateladze Institute of Thermophysics SB RAS,
pr-t Ak. Lavrentieva 1, 630090 Novosibirsk, Russia

Dekterev Alexander,
Kutateladze Institute of Thermophysics SB RAS,
pr-t Ak. Lavrentieva 1, 630090 Novosibirsk, Russia
Siberian Federal University,
79 Svobodny pr., 660041 Krasnoyarsk, Russia

Sentyabov Andrey,
Kutateladze Institute of Thermophysics SB RAS,
pr-t Ak. Lavrentieva 1, 630090 Novosibirsk, Russia
Siberian Federal University,
79 Svobodny pr., 660041 Krasnoyarsk, Russia
Email: Sentyabov_a_v@mail.ru,

Filimonov Sergey,
Kutateladze Institute of Thermophysics SB RAS,
pr-t Ak. Lavrentieva 1, 630090 Novosibirsk, Russia
Siberian Federal University,
79 Svobodny pr., 660041 Krasnoyarsk, Russia